

Publisher: GSA
Journal: GEOL: Geology
Article ID: G24739AR

1 Mantle earthquakes frozen in mylonitized ultramafic
2 pseudotachylytes of spinel-lherzolite facies

3 T. Ueda*¹, M. Obata¹, G. Di Toro², K. Kanagawa³, K. Ozawa⁴

4 [\[\[AU: Please give complete addresses \(including cities and postal codes\).\]\]](#)

5 ¹*Division of Earth and Planetary Sciences, Graduate School of Science, Kyoto University,*
6 *Japan*

7 ²*Dipartimento di Geoscienze, Padova University, Italy*
8 *Istituto Nazionale di Geofisica e Vulcanologia, Rome, Italy*

9 ³*Department of Earth Sciences, Chiba University, Japan*

10 ⁴*Department of Earth and Planetary Sciences, Graduate School of Science, University of*
11 *Tokyo, Japan*

12 *E-mail: t_ueda@kueps.kyoto-u.ac.jp

13 **ABSTRACT**

14 We report a new type of ultramafic pseudotachylyte that forms a fault- and
15 injection-vein network hosted in the mantle-derived Balmuccia peridotite (Italy). In the
16 fault vein the pseudotachylyte is now deformed and recrystallized into a spinel-lherzolite
17 facies ultramylonite, made of a fine (<2 μm) aggregate of olivine, orthopyroxene,
18 clinopyroxene, and spinel, with small amounts of amphibole and dolomite. Electron
19 backscattered diffraction study of the ultramylonite shows a clear crystallographic
20 preferred orientation (CPO) of olivine. The fault vein pseudotachylyte overprints a
21 spinel-lherzolite facies amphibole-bearing mylonite, indicating that shear localization
22 accompanying chemical reaction had taken place in the peridotite before seismic slip

23 produced frictional melting. The occurrence of amphibole in the host mylonite and that of
24 dolomite as well as amphibole in the matrices of ultramylonite and pseudotachylyte may
25 indicate that fluid was present and had evolved in its composition from H₂O-rich to
26 CO₂-rich during ductile deformation with metamorphic reactions, which may account for
27 the observed rheological transition from ductile to brittle behavior. The spinel-lherzolite
28 facies assemblage in mylonites, *P-T* estimations from pyroxene geothermometry and
29 carbonate reactions, and the type of olivine CPO in deformed pseudotachylyte indicate that
30 both the preseismic and the postseismic ductile deformations occurred at ~800 °C and
31 0.7–1.1 GPa.

32 **Keywords:** pseudotachylyte, mantle, peridotite, mylonite, shear localization, earthquake,
33 fluid, dolomite, Balmuccia, Ivrea zone.

34 INTRODUCTION

35 Shear-induced rock melting during earthquakes may occur at mantle depths,
36 according to torsion experiments conducted under high confining pressure (Bridgman,
37 1936) and theoretical studies (e.g., Griggs and Handin, 1960). Kanamori et al. (1998)
38 assumed extensive production of seismic melts during the Mw = 8.3 Bolivian 1994
39 deep-focus (~600 km in depth) earthquake to justify its low seismic efficiency. The product
40 of solidification of seismic melts is pseudotachylyte, which allows us to study the
41 earthquake source mechanics complementary to the seismological one[[AU: Wording?
42 (In particular, is the word “one” ambiguous?)]] (e.g., Sibson, 1975; Di Toro et al.,
43 2005).

44 Ultramafic pseudotachylytes decorate exhumed faults cutting the subcontinental
45 peridotite lenses of Balmuccia (Obata and Karato, 1995) in Italy and the oceanic

46 peridotites in Corsica (Andersen and Austrheim, 2006). Common to these ultramafic
47 pseudotachylytes is the presence of microlites in a glassy matrix (Obata and Karato, 1995;
48 Andersen and Austrheim, 2006). In contrast to the ultramafic pseudotachylytes previously
49 described from the same (Obata and Karato, 1995) and other areas, this study shows
50 evidence for high-temperature mylonitization (in the spinel-lherzolite facies, ~800 °C) of
51 pseudotachylytes, among the highest ever reported. The sequence of events inferred from
52 structural and mineralogical observations supports the possibility of frictional melting and
53 will provide constraints on earthquake nucleation at mantle depths.

54 **GEOLOGIC SETTING**

55 The Balmuccia peridotite is a lenticular mass of spinel lherzolite of 5×0.8 km in
56 size, which is enclosed in an upper amphibolite to granulite facies mafic terrain—the Ivrea
57 zone, northern Italy (see Fig. 1 of Obata and Karato, 1995; the geologic map is also in the
58 [GSA Data Repository Fig. DR1¹](#)). The main lithology of the peridotite massif is spinel
59 lherzolite and spinel harzburgite with porphyroclastic to granoblastic textures (e.g.,
60 Rivalenti et al., 1981; Sinigoi et al., 1983). Layers or dikes of pyroxenite are locally
61 abundant, some of which are folded and cut by faults associated with pseudotachylytes.
62 The peridotite was primarily equilibrated in the mantle at temperature and pressure
63 conditions of $1100\text{ °C} < T < 1200\text{ °C}$ and $1.3\text{ GPa} < P < 2.0\text{ GPa}$, respectively (Shervais,
64 1979). Tectonic emplacement of the peridotite into the continental crust took place during
65 the Carboniferous at 300–320 Ma and was accompanied by high-grade metamorphism at
66 $720\text{ °C} < T < 900\text{ °C}$ and $0.9\text{ GPa} < P < 1.1\text{ GPa}$ (Schmid and Wood, 1976; Handy et al.,
67 1999). The peridotite–mafic granulite complex was first exhumed during the Permian
68 transtension and the early Mesozoic rifting of the Piedmont Ligurian Ocean (Handy and

69 Stünitz, 2002) and then involved in the Tertiary brittle deformation along the Insubric Line
70 during the Alpine collision (Handy et al., 1999).

71 **HOST PERIDOTITES AND PSEUDOTACHYLYTES**

72 Pseudotachylytes, as commonly observed elsewhere (Sibson, 1975), occur **as both**
73 **fault veins** and injection veins, locally forming complex networks in the Balmuccia
74 peridotite. The pseudotachylyte fault veins are typically 1–10 mm thick, straight, and
75 appear black and glassy on fresh surfaces and light yellow on weathered surfaces (see
76 photos in **Fig. DR2**). At the banks along the Sesia River (45°49'12"N, 8°09'12"E), the fault
77 veins are subvertical and strike ~020° and 340°. The sense of shear and finite displacement
78 on these faults may sometimes be determined by the offset of the pyroxenite bands (Fig. 2
79 in Jin et al., 1998).

80 **Host Peridotites**

81 The host rock, away from fault veins, is protogranular coarse-grained spinel
82 lherzolite (with average modal composition, olivine [~60%], orthopyroxene [~25%],
83 clinopyroxene [~10%], and Cr-Al spinel [~5%]; Obata and Karato, 1995). Approaching
84 the fault, wall rocks are progressively deformed and recrystallized (Jin et al., 1998): They
85 form a protomylonite-mylonite consisting of plastically deformed porphyroclasts of
86 olivine, pyroxene, and spinel immersed in a fine-grained (10–50 µm) matrix of
87 recrystallized olivine, orthopyroxene, clinopyroxene, spinel, and pargasitic amphibole
88 (Fig. 1A). Within ~20 cm of the fault, the porphyroclasts are elongated and deflected
89 toward the fault (see a photomicrograph in **Fig. DR3**). Electron microprobe analyses show
90 that recrystallized neoblastic pyroxenes are distinctly less aluminous than the
91 porphyroclastic ones, while olivine is homogeneous (F_{O89-90}) throughout (**Table DR1, Fig.**

92 **DR4**). The amphibole is titaniferous pargasite and typically occurs in fine-grained parts
93 (<60 μm , neoblasts) along grain boundaries of primary large crystals of olivine and
94 pyroxenes.

95 **Pseudotachylyte Fault (i.e., Ultramylonite) and Injection Veins**

96 The fault vein pseudotachylyte is foliated and mylonitized into a fine-grained (<2
97 μm) polymineralic matrix and is formally “ultramylonite” (Fig. 1A). The contact between
98 the wall rock mylonite and the ultramylonite is typically sharp because of the abrupt
99 reduction in grain size and the color contrast (the pseudotachylyte-derived ultramylonite
100 being more brownish in transmitted light; Fig. 1C). Some porphyroclasts in the host
101 mylonite are truncated by the ultramylonite fault vein (Fig. 1A). The ultramylonite
102 contains porphyroclasts of olivine, spinel, orthopyroxene, and clinopyroxene. The sense of
103 shear deduced from the δ -type porphyroclasts (e.g., dextral in Fig. 1B) in the fault vein is
104 consistent with that deduced from dike separations, with shape-preferred orientation (SPO)
105 in the ultramylonite matrix and with the deflection in the host mylonite.

106 The presence of an injection vein connected to the main ultramylonite shear band
107 (Fig. 1C; **Fig. DR2**) does suggest that the ultramylonite was originally a pseudotachylyte of
108 melt origin. While the main shear zone is foliated, the injection and the pockets are largely
109 massive but locally contain a weak foliation defined by the alignment of elongated olivine
110 clasts, subparallel to the injection wall and at high angles to the main fault vein.

111 Scanning electron microscope (SEM) investigations of the pseudotachylyte
112 revealed that both the fault and injection vein materials are holocrystalline, very
113 fine-grained (<2 μm) and equigranular to subequigranular, consisting of olivine,
114 orthopyroxene, clinopyroxene, and spinel, with small amounts (a few volume percent) of

115 amphibole and dolomite. Dolomite and amphibole **were** identified by a combination of
116 electron backscattered diffraction (EBSD) pattern and semiquantitative X-ray
117 spectroscopy. Dolomite is ubiquitous in the pseudotachylyte, both in the fault vein and in
118 the injection vein; it appears as dark phase in backscattered electron (BSE) images (Figs.
119 2A and 2B). An accurate modal amount of the amphibole is difficult to estimate in BSE
120 images but is probably less than a few percent according to EBSD analysis and
121 compositional mapping by X-ray spectroscopy. Olivine, pyroxene, amphibole, and
122 dolomite are texturally and thus chemically in equilibrium (Fig. 2A). In addition, the
123 injection veins contain numerous nanoparticles of Fe-Ni sulfide (as identified by
124 energy-dispersive X-ray spectroscopy [EDS])**[[AU: Can this be changed to**
125 **“energy-dispersive spectrometry [EDS]” or “energy-dispersive X-ray fluorescence**
126 **[EDS-XRF]” (per GSA style)?]]** along the grain boundaries, while the sulfide grains are
127 sparse and coarser-grained in the mylonitized fault vein. A shape-preferred orientation
128 (SPO) was observed in an injection vein at high **magnification** (Fig. 2A). The lack of
129 obvious SPO in the fault vein may be ascribed to more extensive recrystallization during
130 the postseismic shear. The SPO is subparallel to the wall of the injection vein and at high
131 angles to the fault vein. Furthermore, the fault vein has a clear crystallographic preferred
132 orientation (CPO) of olivine as described below.

133 **CRYSTALLOGRAPHIC PREFERRED ORIENTATION (CPO) OF OLIVINE**

134 Crystallographic orientations of olivine in the fault vein pseudotachylyte (i.e.,
135 ultramylonite) were studied using the EBSD technique. Measurements were made on a thin
136 section cut orthogonal to the fault foliation and parallel to the lineation, using a JEOL
137 JSM-6460 SEM (Chiba University) and a JEOL 7000F FE-SEM (University of Tokyo)

138 operating at 15–20 kV and 5–9 nA. Data were processed using HKL Channel-5 software
139 (Flamenco). Because of the small grain size (mostly less than 1 μm in diameter), indexing
140 of electron diffraction pattern together with phase identification was made manually on
141 each beam spot. The results are plotted in Figure 3.

142 Olivine exhibits a CPO with [100] axes subparallel to the lineation and [010] axes
143 subperpendicular to the foliation (Fig. 3) rather similar to the A-type fabric of Jung and
144 Karato (2001), which may indicate an activation of the (010)[100][[AU: OK? (As
145 opposed to “[010][100]” or “[010]-[100]”?)]] slip system in olivine (Carter and
146 Ave’Lallemant, 1970), suggesting a significantly high-temperature ductile deformation
147 within the fault vein.

148 The host, coarse-grained peridotite, remote from the fault vein, also has the A-type
149 CPO pattern, but with a distinct orientation of maxima from that of the mylonitized
150 pseudotachylyte (see Fig. 8 in Jin et al., 1998). The olivine CPO of protomylonite becomes
151 diffuse as the fault is approached, a result of the recrystallized fine-grained olivine having a
152 different CPO pattern from the porphyroclasts as seen in Figure 8B of Jin et al. (1998), i.e.,
153 a strong [001] maximum and diffuse [100] and [010] peaks. The latter is distinct from the
154 CPO we observed in the mylonitized pseudotachylyte.

155 **DISCUSSION**

156 **Sequence of Deformation and Crystallization Events**

157 From textural observation the sequence of events in the shear zone is inferred as
158 follows: (1) shear localization and recrystallization of host peridotite (that involve
159 hydration, i.e., the amphibole formation), producing a narrow mylonite zone, (2) a seismic
160 rupture and slip in or around the mylonite zone, which resulted in frictional melting and the

161 formation of pseudotachylyte, and (3) a further shear *within* the pseudotachylyte vein,
162 producing an ultramylonite. The deflection of the ultramylonite foliation at the mouth of
163 the injection vein (Fig. 1C) may indicate that flowing material was still hot and fluidal
164 during a residual shear of the main seismic slip and melting. The high-temperature CPO
165 (Fig. 3) is consistent with this inference. Petrological and mineralogical observations
166 indicate that this sequence of event took place under spinel-lherzolite facies conditions.

167 The preseismic ductile shear that produced the host mylonite was probably a slow
168 and long-lasting ductile deformation event, because the dominant mechanism of the
169 deformation is thought to be the dislocation creep coupled with metamorphic reactions,
170 which are governed by diffusive processes both in the solid and along grain boundaries.
171 Seismic rupture, on the other hand, involves rapid displacement (of the rate 1–5 m/s) and
172 rupture velocities (1–4 km/s; Scholz, 2002).

173 The observed transition from ductile shear to seismic rupture is puzzling because
174 ductile shear localization suggests strain softening (e.g., Jin et al., 1998), while seismic
175 rupture indicates a substantial stress accumulation. The association of pseudotachylyte and
176 mylonite has been observed in many localities (e.g., Sibson, 1980 **[[Q1: The in-text
177 citation "Sibson, 1980" is not in the reference list. Please correct the citation, add the
178 reference to the list, or delete the citation. Q1]]**; Passchier, 1982; White, 1996, 2004),
179 for which different interpretations have been proposed (e.g., Sibson, 1980 **[[Q2: The
180 in-text citation "Sibson, 1980" is not in the reference list. Please correct the citation,
181 add the reference to the list, or delete the citation. Q2]]**; Hobbs et al., 1986; White,
182 1996, 2004; Kelemen and Hirth, 2007). Because of the occurrence of amphibole in the
183 neoblasts in host mylonite and the ubiquity of dolomite in the pseudotachylyte, we infer

184 that fluid had evolved in composition during the preseismic ductile shearing and played an
185 important role in such a rheological transition.

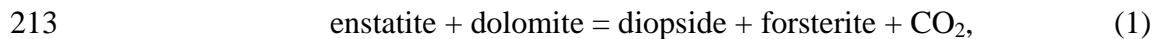
186 **Fluid Chemistry Evolution and Consequences on Rock Strength**

187 We suppose that a fluid introduced in the shear zone originally contained CO₂ as
188 well as H₂O. The introduction of fluid and the progress of shear deformation may have
189 occurred concomitantly and cooperatively because metamorphic reactions and
190 recrystallization would enhance the rock ductility (e.g., White and Knipe, 1978). The
191 formation of amphibole in metamorphic reactions consumes H₂O, making the residual
192 fluid progressively enriched with CO₂ if the supply of a new fluid is limited or delayed.
193 The CO₂ enrichment in the fluid would reduce the connectivity of the fluid because of the
194 increase of fluid dihedral angle, thereby reducing the permeability (Watson and Brenan,
195 1987; Riley and Kohlstedt, 1990), thus impeding an external supply of additional H₂O-rich
196 fluid. The fluid-circulating system thus becomes unstable and will eventually become
197 closed due to the permeability loss. Once the system becomes closed, it will continue being
198 so until some catastrophic structural change such as rupture occurs. The ubiquity of
199 dolomite in the pseudotachylyte can suggest that the activity of H₂O was not internally
200 buffered during the preseismic metamorphism. The reduction of H₂O activity will cause a
201 hardening of olivine due to reduction of point defects (Karato et al., 1986). Thus the
202 reaction-controlled chemical evolution of the fluid from H₂O-rich to CO₂-rich likely
203 results in a strain hardening in the shear zone.

204 **Ambient Conditions During Deformation**

205 The temperature of the preseismic deformation was estimated to be ~800 °C by
206 applying the Ca-Mg exchange pyroxene geothermometer (Taylor, 1988) to the microprobe

207 analyses of the neoblastic pyroxenes in the host mylonite (Table DR1), and we consider
208 this representing the ambient condition of the seismic event. Given the grain size (<2 μm)
209 of the mylonitized pseudotachylyte vein, too small for microprobe analyses, we used the
210 dolomite-enstatite equilibria to estimate the *postseismic* ambient conditions. The
211 dolomite-enstatite stability field is bounded at high temperatures by the decarbonate
212 reaction (Fig. 4) (Brey et al., 1983),



214 and at the low temperature by the reaction,



216 Note that reaction 2 is a CO₂-conserving reaction, and therefore it is independent of
217 the activity of CO₂. Considering the variability of the activities of H₂O and CO₂, it is
218 conceivable that the preseismic and postseismic recrystallizations share the same *P-T*
219 regime. It follows that pseudotachylyte were produced at ambient conditions of ~800 °C
220 and 0.7–1.1 GPa (Fig. 4). Given the exhumation history of the Balmuccia peridotite, this
221 *P-T estimate* would correspond to continental, lower-crust, or, probably (e.g., Fig. 11 in
222 Handy and Stünitz, 2002), upper-mantle deformation conditions.

223 CONCLUSIONS

224 Microstructural and mineralogical observations of an ultramafic mylonitized
225 pseudotachylyte have provided information about the seismic cycle at lower-crust or
226 upper-mantle conditions. The cycle includes initial fluid-assisted ductile shear localization
227 (producing host mylonite), followed by a seismic slip (producing pseudotachylyte), and
228 further ductile shear (producing ultramylonite). All these deformation events took place in
229 the spinel-lherzolite stability field (~800 °C and 0.7–1.1 GPa). Such high-temperature

230 deformation conditions preclude the formation or the preservation of glasses or quench
231 textures typically observed in more common shallow-seated pseudotachylytes, which
232 makes the recognition of pseudotachylytes difficult in high-grade terrains. Identification
233 and detailed study of such mylonitized pseudotachylytes remains an important task for
234 further study of earthquake mechanics in the upper mantle.

235 **ACKNOWLEDGMENTS**

236 We thank Greg Hirth, Joe Clancy White, and an anonymous reviewer for their
237 detailed comments to improve the manuscript. Ueda, Obata, and Di Toro thank T.
238 Shimamoto and A. Tsutsumi for many discussions and encouragements, and T. Hirose
239 for supplying some critical sample and field information. Di Toro thanks O. Fabbri and
240 G. Pennacchioni for field support; Ueda and Obata thank H. Nagahara for the use of
241 FE-SEM at Tokyo, and H. Yoshida for his technical assistance. Obata thanks F. Seifert
242 and Bayerisches Geoinstitut (University of Bayreuth) for financially supporting the
243 fieldwork in 1993. Kanagawa was supported by **JSPS** grant 17340159, and Di Toro by
244 **PRIN** grant 2005044945 and a **CARIPARO** grant. **[[AU: Regarding the three**
245 **acronyms: please spell out.]]**

246 **REFERENCES CITED**

247 Andersen, T.B., and Austrheim, H., 2006, Fossil earthquakes recorded by
248 pseudotachylytes in mantle peridotite from the Alpine subduction complex of Corsica:
249 Earth and Planetary Science Letters, v. 242, p. 58–72, doi:
250 10.1016/j.epsl.2005.11.058.

- 251 Brey, G., Brice, W.R., Ellis, D.J., Green, D.H., Harris, K.L., and Ryabchikov, I.D., 1983,
252 Pyroxene-carbonate reactions in the upper mantle: *Earth and Planetary Science*
253 *Letters*, v. 62, p. 63–74, doi: 10.1016/0012-821X(83)90071-7.
- 254 Bridgman, P.W., 1936, Shearing phenomena at high pressure of possible importance for
255 geology: *Journal of Geology*, v. 44, p. 653–669.
- 256 Carter, N.L., and Ave'Lallemant, H.G., 1970, High temperature flow of dunite and
257 peridotite: *Geological Society of America Bulletin*, v. 81, p. 2181–2202, doi:
258 10.1130/0016-7606(1970)81[2181:HTFODA]2.0.CO;2.
- 259 Di Toro, G., Nielsen, S., and Pennacchioni, G., 2005, Earthquake rupture dynamics frozen
260 in exhumed ancient faults: *Nature*, v. 436, p. 1009–1012, doi: 10.1038/nature03910.
- 261 Gasparik, T., 1984, Two-pyroxene thermobarometry with new experimental data in the
262 system CaO-MgO-Al₂O₃-SiO₂: *Contributions to Mineralogy and Petrology*, v. 87,
263 p. 87–97, doi: 10.1007/BF00371405.
- 264 Griggs, D., and Handin, J., 1960, Observations on fracture and a hypothesis of
265 earthquakes: *Geological Society of America Memoir* 79, p. 343–373.
- 266 Handy, M.R., and Stünitz, H., 2002, Strain localization by fracturing and reaction
267 weakening—A mechanism for initiating exhumation of subcontinental mantle
268 beneath rifted margins, *in* de Meer, S., et al., eds., *Deformation mechanisms, rheology*
269 *and tectonics: Current status and future perspectives: The Geological Society of*
270 *London Special Publication 200*, p. 387–407.
- 271 Handy, M.R., Franz, L., Heller, F., Janott, B., and Zurbriggen, R., 1999, Multistage
272 accretion and exhumation of the continental crust (Ivrea crustal section, Italy and
273 Switzerland): *Tectonics*, v. 18, p. 1154–1177, doi: 10.1029/1999TC900034.

- 274 Hobbs, B.E., Ord, A., and Teyssier, C., 1986, Earthquakes in the ductile regime?: Pure and
275 Applied Geophysics, v. 124, p. 309–335, doi: 10.1007/BF00875730.
- 276 Jin, D., Karato, S., and Obata, M., 1998, Mechanisms of shear localization in the
277 continental lithosphere: Inference from the deformation microstructures of peridotites
278 from the Ivrea zone, northwestern Italy: Journal of Structural Geology, v. 20,
279 p. 195–209, doi: 10.1016/S0191-8141(97)00059-X.
- 280 Jung, H., and Karato, S., 2001, Water-induced fabric transitions in olivine: Science, v. 293,
281 p. 1460–1463, doi: 10.1126/science.1062235.
- 282 Kanamori, H., Anderson, D.L., and Heaton, T.H., 1998, Frictional melting during the
283 rupture of the 1994 Bolivian earthquake: Science, v. 279, p. 839–842, doi:
284 10.1126/science.279.5352.839.
- 285 Karato, S., Paterson, M.S., and Fitz Gerald, J.D., 1986, Rheology of synthetic olivine
286 aggregates—Influence of grain size and water: Journal of Geophysical Research,
287 v. 91, p. 8151–8176, doi: 10.1029/JB091iB08p08151.
- 288 Kelemen, P.B., and Hirth, G., 2007, A periodic shear-heating mechanism for
289 intermediate-depth earthquakes in the mantle: Nature, v. 446, p. 787–790, doi:
290 10.1038/nature05717.
- 291 Obata, M., and Karato, S., 1995, Ultramafic pseudotachylite from the Balmuccia
292 peridotite, Ivrea-Verbanò zone, northern Italy: Tectonophysics, v. 242, p. 313–328,
293 doi: 10.1016/0040-1951(94)00228-2.
- 294 Passchier, C.W., 1982, Pseudotachylite and the development of ultramylonite bands in the
295 Saint-Barthelémy Massif, French Pyrenees: Journal of Structural Geology, v. 4,
296 p. 69–79, doi: 10.1016/0191-8141(82)90008-6.

- 297 Riley, G.N., Jr., and Kohlstedt, D.L., 1990, Melt migration in a silicate liquid-olivine
298 system: An experimental test of compaction theory: *Geophysical Research Letters*,
299 v. 17, no. 12, p. 2101–2104, doi: 10.1029/GL017i012p02101.
- 300 Rivalenti, G., Garuti, G., Rossi, A., Siena, F., and Sinigoi, S., 1981, Existence of different
301 peridotite types and of a layered igneous complex in the Ivrea zone of the western
302 Alps: *Journal of Petrology*, v. 22, p. 127–153.
- 303 Schmid, R., and Wood, B.J., 1976, Phase relationships in granulitic metapelites from the
304 Ivrea-Verbano zone (northern Italy): *Contributions to Mineralogy and Petrology*,
305 v. 54, p. 255–279, doi: 10.1007/BF00389407.
- 306 Scholz, C.H., 2002, *The mechanics of earthquakes and faulting* (2nd edition): Cambridge,
307 UK, Cambridge University Press, 471 p.
- 308 Shervais, J.W., 1979, Thermal emplacement model for the alpine lherzolite massif at
309 Balmuccia, Italy: *Journal of Petrology*, v. 20, p. 795–820.
- 310 Sibson, R.H., 1975, Generation of pseudotachylyte by ancient seismic faulting:
311 *Geophysical Journal of the Royal Astronomical Society*, v. 43, p. 775–794.
- 312 Sinigoi, S., Comin-Chiaramonti, P., Demarchi, G., and Siena, F., 1983, Differentiation of
313 partial melts in the mantle: Evidence from the Balmuccia peridotite, Italy:
314 *Contributions to Mineralogy and Petrology*, v. 82, p. 351–359, doi:
315 10.1007/BF00399712.
- 316 Taylor, W.R., 1988, An experimental test of some geothermometer and geobarometer
317 formulations: *Neues Jahrbuch für Mineralogie*, v. 172, p. 381–408.
- 318 Watson, E.B., and Brenan, J.M., 1987, *Fluids in the lithosphere*, 1: Experimentally
319 determined wetting characteristics of CO₂-H₂O fluids and their implications for fluid

320 transport, host-rock physical properties, and fluid inclusion formation: Earth and
321 Planetary Science Letters, v. 85, p. 497–515, doi: 10.1016/0012-821X(87)90144-0.
322 White, J.C., 1996, Transient discontinuities revisited: Pseudotachylyte, plastic instability
323 and the influence of low pore fluid pressure on deformation processes in the mid-crust:
324 Journal of Structural Geology, v. 18, p. 1471–1486.
325 White, J.C., 2004, Instability and localization of deformation in lower crust granulites,
326 Minas fault zone, Nova Scotia, Canada: **The Geological Society of London Special**
327 **Publication 224**, p. 25–37, doi: 10.1144/GSL.SP.2004.224.01.03.
328 White, S.H., and Knipe, R.J., 1978, Transformation- and reaction-enhanced ductility in
329 rocks: **The Geological Society of London Journal**, v. 135, p. 513–516.

330 **FIGURE CAPTIONS**

331 Figure 1. Optical images of the mylonitized pseudotachylyte. A: The wall rock
332 protomylonite (bottom) truncated by the ultramylonite (= mylonitized pseudotachylyte
333 fault vein, top). Cross-polarized light. B: Porphyroclastic system of spinel in the
334 mylonitized pseudotachylyte. The wings of stable spinel indicate high-temperature
335 deformation during postseismic deformation (see text). Fault plane is horizontal.
336 Plane-polarized light. C: Injection vein and pockets (black arrows) originated from
337 mylonitized pseudotachylyte fault vein. Pseudotachylyte pockets probably connected to
338 the fault vein, judging from observation of multiple thin sections of the same sample. Thin
339 white “ribbon” (white arrow) in the fault vein is elongated tail of clasts. Light-colored thick
340 bands labeled “Cl.” are slices of host protomylonite. Red ellipse indicates the layer from
341 which CPO data (Fig. 3) were obtained. Sinistral shear. Plane-polarized light. Sample
342 VS14.

343

344 Figure 2. BSE image of an injection vein (A) and a fault vein pseudotachylyte (B) (sample
345 VS14) obtained at 15 keV. The direction of the fault plane is parallel to the short side of
346 photographs. Dol—dolomite; Sp—spinel; Sul—sulfide.

347

348 Figure 3. Pole figures of crystallographic orientations of olivine (axes [100], [010], and
349 [001]) in a mylonitized pseudotachylyte, obtained by EBSD. The data were obtained from
350 another thin section of the same sample (VS14); red ellipse in Figure 1C indicates the
351 relevant layer from which the EBSD data were obtained. Foliation is horizontal (XY plane,
352 solid line) with lineation (X). The shear sense is indicated by arrows on the top right.

353 Equal-area, lower-hemisphere projections. The gray shading is calculated with Gaussian
354 half-width of 15° referring to the density of data points (n = 164); the numbers in the legend
355 correspond to **[[AU: Should this be “are”?]]** the multiples of uniform distribution density.
356 A color version of the same diagram is given in Fig. DR4 (see footnote 1).

357

358 Figure 4. Ambient *P-T* condition for deformation of the wall rock (gray band) and of the
359 pseudotachylyte vein (area between thick lines; see text). Temperature obtained by
360 pyroxene geothermometer is indicated by a dashed line (the gray band includes the error).
361 Lherzolite facies boundaries (for CaO-MgO-Al₂O₃-SiO₂ system) after Gasparik (1984).
362 Reaction lines of carbonate (see text) after Brey et al. (1983). Di—diopside; En—enstatite;
363 Fo—forsterite.

364

365 ¹GSA Data Repository item 2008##, Figure DR1 (geologic map), Figure DR2 (field
366 photographs of fault vein pseudotachylytes), Figure DR3 (photomicrograph showing
367 deflection of the structure of host peridotite [sample 9310]), Figure DR4 (color version of
368 Figure 3), and Table DR1 (microprobe analyses of mineral), is available online at
369 www.geosociety.org/pubs/ft2008.htm, or on request from editing@geosociety.org or
370 Documents Secretary, GSA, P.O. Box 9140, Boulder, CO 80301, USA.